The effect of Al/Si ratio on the transport properties of the layered intermetallic compound $CaAl_2Si_2$

2007 J. Phys.: Condens. Matter 19 176206

(http://iopscience.iop.org/0953-8984/19/17/176206)

IOP PUBLISHING JOURNAL OF PHYSICS: CONDENSED MATTER

J. Phys.: Condens. Matter **19** (2007) 176206 (10pp) doi:10.1088/0953-8984/19/17/176206

The effect of Al/Si ratio on the transport properties of the layered intermetallic compound $CaAl_2Si_2$

Y K Kuo[1], K M Sivakumar[1], J I Tasi[1], C S Lue[2], J W Huang[2], S Y Wang[2], Dinesh Varshney[3], N Kaurav[3] and R K Singh[4]

[1] Department of Physics, National Dong Hwa University, Hualien 97401, Taiwan
[2] Department of Physics, National Cheng Kung University, Tainan 70101, Taiwan
[3] School of Physics, Devi Ahilya University, Khandwa Road Campus, Indore 452001, India
[4] Institute of Professional and Scientific Studies and Research, Chaudhary Devi Lal University, Sirsa, Harayana 125055, India

E-mail: ykkuo@mail.ndhu.edu.tw and cslue@mail.ncku.edu.tw

Received 3 February 2007, in final form 1 March 2007
Published 28 March 2007
Online at stacks.iop.org/JPhysCM/19/176206

Abstract

We report the results of the electrical resistivity and Seebeck coefficient as well as thermal conductivity measurements on the stoichiometric $CaAl_2Si_2$ and non-stoichiometric $CaAl_{1.75}Si_{2.25}$, $CaAl_{1.9}Si_{2.1}$, $CaAl_{2.1}Si_{1.9}$, and $CaAl_{2.25}Si_{1.75}$ compounds in the temperature range 10–300 K. It has been found that the magnitude of electrical resistivity decreases for the non-stoichiometric samples, attributed to the shift of Fermi energy from the dip of the density of states as a consequence of the changed Si/Al content. In addition, a systematic change in the magnitude of Seebeck coefficient as a function of Al/Si concentration has been observed. The results have been associated with the effect of hole/electron doping on the Fermi level density of states. A detailed analysis of the electrical resistivity and Seebeck coefficient suggests the presence of two types of charge carrier and the temperature dependent changes in their mobility. From the thermal conductivity results, we correlated the extent of disorder and Al/Si ratio with various thermal scattering mechanisms in the investigated temperature range.

1. Introduction

Binary and ternary silicides are well known for their diverse physical properties depending on the composition/constituent elements as a consequence of the corresponding changes in their electronic structure. Recently, the layered intermetallic ternary alumino-silicides Ca–Al–Si have attracted considerable attention [1–6] after the discovery of MgB_2, which is also a layered compound with a substantially high superconducting transition temperature T_c of 39 K [7]. There are two types of layered ternary Ca-based alumino-silicide: CaAlSi, isostructural to

MgB_2, is a superconductor with $T_c \sim 7.8$ K [1, 2], and $CaAl_2Si_2$ is a nonsuperconducting semimetal [3, 4].

The titled compound $CaAl_2Si_2$, relatively little studied, has the La_2O_3-type layered trigonal structure (space group: $P\bar{3}M1$), where Al and Si atoms are arranged in chemically ordered double-corrugated hexagonal layers and Ca atoms are intercalated between them [3]. A recent Hall coefficient measurement on single-crystalline $CaAl_2Si_2$ exhibited a sign reversal at around 150 K, indicating that the dominant carrier changes with temperature [3]. According to the electronic structure calculations, $CaAl_2Si_2$ is a semimetal arising from a slight overlap of one conduction band and two valence bands, with the Fermi level (E_F) located at the valley of the density of states (DOS) [4, 5]. Hence, the observed phenomena in the transport properties of $CaAl_2Si_2$ have been attributed to the semimetallic response, based on the calculated band feature.

To shed more light on the physical properties of $CaAl_2Si_2$, an investigation of the composition variation by a variety of physical quantities would be instructive. In this work, we thus performed the electrical resistivity (ρ) and Seebeck coefficient (S) as well as thermal conductivity (κ) measurements on $CaAl_{2-x}Si_{2+x}$ with $-0.25 \leqslant x \leqslant +0.25$ in the temperature range 10–300 K. It is well known that S is very sensitive to the composition dependent variations in the electronic structure, especially for the systems with E_F located at the dip of the DOS. Also the thermal conductivity yields useful information about the changes in the temperature dependent phonon–phonon and electron–phonon scattering. Further, as a complementary tool to the Hall coefficient, S can be effectively employed to investigate the temperature variation in the type of charge carrier and/or mobility. In this study, the result of the Seebeck coefficient shows a noticeable composition dependence on both sign and magnitude, suggesting a considerable modification in the Fermi level DOS with respect to the Al/Si ratio change.

2. Experiment

Polycrystalline samples were prepared by arc-melting high purity elements under argon atmosphere. To promote homogeneity, the resulting ingots were annealed in a vacuum-sealed quartz tube at 800 °C for two days, followed by furnace cooling. An x-ray analysis taken with Cu Kα radiation on the powder specimens shows a single phase. All reflection peaks in the diffraction spectra could be indexed according to the expected La_2O_3-type structure. Electrical resistivity data were obtained by a standard four-probe method. Seebeck coefficient and thermal conductivity measurements were simultaneously carried out in the helium closed cycle refrigerator using a heat pulse technique. A detailed description of these experimental techniques can be found elsewhere [8].

3. Results and discussion

3.1. Electrical resistivity

The temperature dependence of the electrical resistivity $\rho(T)$ of the $CaAl_{2-x}Si_{2+x}$ alloys from 10 to 300 K is shown in figure 1. For the stoichiometric compound $CaAl_2Si_2$, ρ increases slightly with rising temperature, tends to saturate at around 200 K, and then starts decreasing upon further heating. The observed $\rho(T)$ feature is similar to that earlier reported [3]. The relatively large magnitude and the high-temperature variation of the electrical resistivity are reminiscent of a semimetal. For the non-stoichiometric samples, the electrical resistivity decreases with respect to $CaAl_2Si_2$, attributed to the enhancement of the carrier density as a

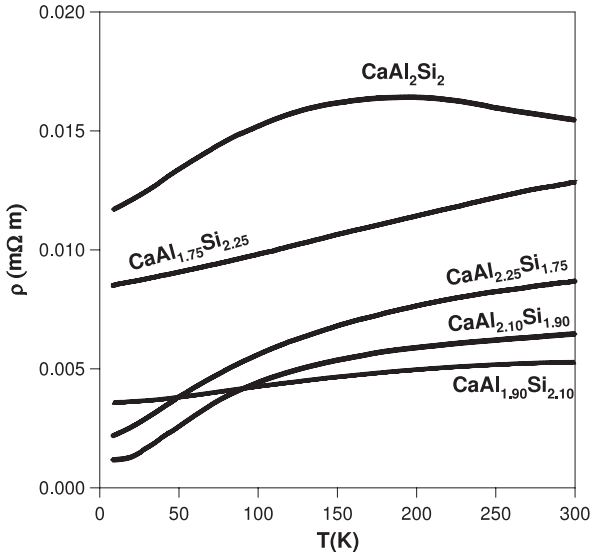

Figure 1. Electrical resistivity of $CaAl_{1.75}Si_{2.25}$, $CaAl_{1.9}Si_{2.1}$, $CaAl_2Si_2$, $CaAl_{2.1}Si_{1.9}$, and $CaAl_{2.25}Si_{1.75}$.

consequence of the shift of E_F from the valley of the DOS to higher positions. In addition, two distinct $\rho(T)$ characteristics could be established for various Si/Al ratios. For the Al deficient samples ($CaAl_{1.75}Si_{2.25}$ and $CaAl_{1.9}Si_{2.1}$), $\rho(T)$ exhibits a weak linear temperature dependence, typical semimetallic behaviour. On the other hand, the Al excess samples ($CaAl_{2.1}Si_{1.9}$ and $CaAl_{2.25}Si_{1.75}$) show metallic characteristics with lower residual resistivity. These results can be understood in terms of the rigid-band scenario, which is further supported by the Seebeck coefficient results, and will be discussed later.

To have a quantitative viewpoint of the measured results, the electrical transport data of $CaAl_2Si_2$ were analysed theoretically. The temperature-dependent electrical resistivity is generally expressed as

$$\rho \approx \left(\frac{3}{\hbar e^2 v_F^2}\right)\frac{k_B T}{M v_s^2}\int_0^{2k_F} |v(q)|^2 \left[\frac{(\hbar\omega/k_B T)^2 q^3\,\mathrm{d}q}{(\exp(\hbar\omega/k_B T)-1)(1-\exp(-\hbar\omega/k_B T))}\right]. \tag{1}$$

Here $v(q)$ is the Fourier transform of the potential associated with one lattice site and v_s is the sound velocity. Equation (1) in terms of the acoustic phonon contribution yields the Bloch–Gruneisen function for the temperature-dependent resistivity [9]:

$$\rho_{ac}(T,\theta_D) = 4A_{ac}(T/\theta_D)^4 \times T\int_0^{\theta_D/T} x^5(e^x-1)^{-1}(1-e^{-x})^{-1}\,\mathrm{d}x, \tag{2}$$

where $x = \hbar\omega/k_B T$ and A_{ac} is a constant of proportionality. We further assume that the modelled phonon spectrum consists of two parts: an acoustic Debye branch characterized by the Debye temperature θ_D and an optical peak defined by the Einstein temperature θ_E. In the case of the Einstein type of phonon spectrum (an optical mode), $\rho_{op}(T)$ can be described as follows:

$$\rho_{op}(T,\theta_E) = A_{op}\theta_E^2 T^{-1}[\exp(\theta_E/T)-1]^{-1} \times [1-\exp(-\theta_E/T)]^{-1}. \tag{3}$$

Here A_{op} is defined analogously to equation (2). Thus, the phonon resistivity can be conveniently modelled by combining both terms arising from acoustic and optical phonons

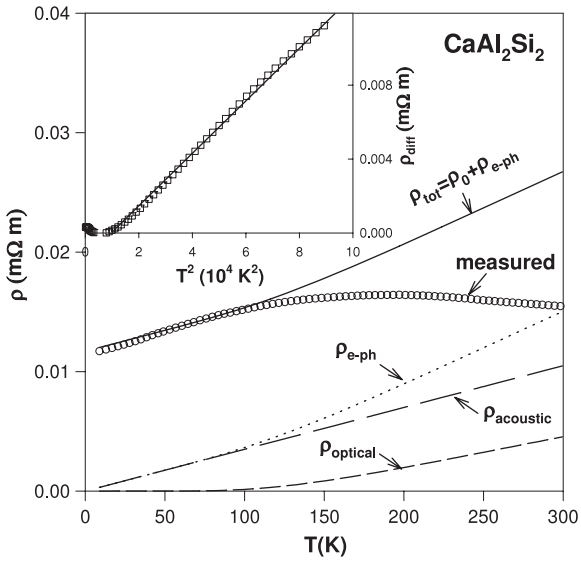

Figure 2. Variation of ρ_{e-ph} with temperature for $CaAl_2Si_2$ and the contribution of acoustic phonons ρ_{ac} as well of optical phonons ρ_{op} to the resistivity. The calculated ρ_{tot} $(= \rho_0 + \rho_{e-ph})$ deviates from the measured data (closed circles) above 120 K. The inset shows the variation of ρ_{diff} $(=\rho_{exp} - \rho_{tot})$ versus T^2; a linear dependence above 120 K is clearly seen.

$$\rho_{e-ph}(T) = \rho_{ac}(T, \theta_D) + \rho_{op}(T, \theta_E). \tag{4}$$

If the Matthiessen rule is obeyed, the resistivity may be represented as a sum $\rho_{tot}(T) = \rho_0 + \rho_{e-ph}(T)$, where ρ_0 is the temperature-independent residual resistivity. The resistivity curves plotted in figure 2 manifest that parts of resistivity were determined by the electron scattering on acoustic and optical phonons, shown along with the total phonon resistivity. As inferred from the curve, ρ_{ac} increases rather linearly while ρ_{op} exhibits an exponential growth with temperature. Here $\theta_D = 274$ K and $\theta_E = 542$ K were taken from the reported band structure calculation on $CaAl_2Si_2$ [5]. The deduced numerical results on the temperature dependence of resistivity of $CaAl_2Si_2$ are also given in figure 2 along with the experimental data. The significant feature is that the estimated ρ is quite consistent with the experimental data at lower temperatures, but starts to deviate from the data above $T \sim 120$ K. The difference between the calculated and measured electrical resistivity $\rho_{diff}[= (\rho_0 + \rho_{e-ph}) - \rho_{exp}]$ against T^2 is plotted in the inset of figure 2, where a linear variation is clearly seen above 120 K. Such a power law dependence of ρ_{diff} (quadratic in temperature) at higher temperatures is an indication of electron–electron scattering. The additional term due to the electron–electron contribution was required in understanding the resistivity behaviour, as extensive attempts to fit the data with residual resistivity and phonon resistivity were unsuccessful. The power temperature dependence of ρ_{dif} with electron–electron scattering was also earlier noticed in copper oxides [10], bismuth oxides [11], doped fullerides [12], and sulfides like TiS_2 [13]. The departure from electron–phonon induced resistivity behaviour could be ascribed to either the change in dimensionality or the change in carrier density/mobility. It is worth pointing out that in the Hall coefficient measurement [1], the type of dominant carrier was found to be varying from electron-like to hole-like below 150 K together with peculiar transport properties. Such observations in the electrical transport properties have been associated with the typical response

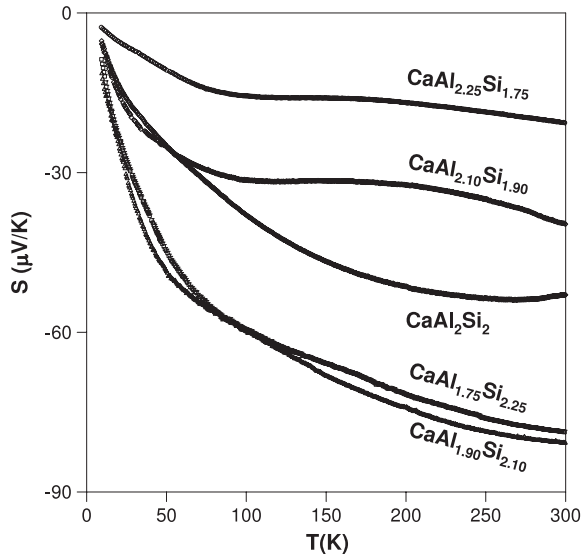

Figure 3. Seebeck coefficient as a function of temperature for the $CaAl_{1.75}Si_{2.25}$, $CaAl_{1.9}Si_{2.1}$, $CaAl_2Si_2$, $CaAl_{2.1}Si_{1.9}$, and $CaAl_{2.25}Si_{1.75}$ alloys.

for an ordinary semimetal. Our analysis of the electrical resistivity of $CaAl_2Si_2$ suggests that besides electron–phonon another possibility for the change in carrier density arose due to the presence of electron correlation.

3.2. Seebeck coefficient

The plot of $S(T)$ of $CaAl_{2-x}Si_{2+x}$ from 10 to 300 K is displayed in figure 3. In the currently investigated alloys, the Seebeck coefficients were found to be negative in the entire temperature range under investigation, suggesting that the electron-type carriers dominate the thermoelectric transport. The off-stoichiometric effect clearly indicates that the magnitude of S is enhanced for the Al-deficient samples while S is reduced for the Si-deficient ones. Similar to the observations from electrical resistivity measurements, two distinct $S(T)$ characteristics appear between the Al-poor and Si-poor samples. The earlier report of Hall coefficient has revealed a sign reversal from negative to positive below 150 K in $CaAl_2Si_2$, attributed to the change of carrier concentration and/or mobility with the temperature [3]. The absence of such a sign reversal in S could be due to other factors associated with the position of E_F in the electronic DOS. Unlike electrical resistivity, which is directly proportional to the Fermi-level density of states $N(E_F)$, the Seebeck coefficient is related to the energy derivative at E_F. Therefore, the sign and magnitude of S strongly depend on the position of E_F in the DOS in addition to the carrier type and concentration [14, 15]. It could be that the $\partial N(E)/\partial E$ has a stronger effect than $N(E_F)$ itself, which predominates the sign of the measured Seebeck coefficient in the present case.

The observed composition variation in S can be interpreted in terms of the rigid-band model with a shift of E_F corresponding to the change of x in $CaAl_{2-x}Si_{2+x}$. As Si has one more electron in its valence shell than Al, a partial replacement of Al by Si is expected to dump electrons in the conduction band, leading to an upward shift of E_F with respect to $CaAl_2Si_2$. It thus enhances the electron pocket but reduces the hole ones. As a result, the negative S values for $CaAl_{1.75}Si_{2.25}$ and $CaAl_{1.9}Si_{2.1}$ increase as compared to that of $CaAl_2Si_2$. On the other hand, a partial replacement of Si by Al will cause a downward shift of E_F, resulting in a reduction of

Table 1. Fitting parameters of Seebeck coefficient determined from equations (5)–(7).

Samples	c_e (eV^{-1})	ε (meV)	E_h (meV)
$CaAl_{1.75}Si_{2.25}$	0.2	45.41	52.52
$CaAl_{1.9}Si_{2.1}$	0.21	44.17	53.46
$CaAl_2Si_2$	0.16	57.0	65.35
$CaAl_{2.1}Si_{1.9}$	0.46	97.1	45.00
$CaAl_{2.25}Si_{1.75}$	0.43	97.38	45.67

the electron pocket but an enhancement of the hole ones. Therefore, the negative S values for $CaAl_{2.25}Si_{1.75}$ and $CaAl_{2.1}Si_{1.9}$ decrease as observed.

It is worthwhile mentioning that a preliminary ^{27}Al NMR measurement on $CaAl_{2-x}Si_{2+x}$ also exhibits a similar tendency [16]. From NMR spin–lattice relaxation rates, a larger Al s Fermi-level DOS in $CaAl_{2.1}Si_{1.9}$ and a smaller one in $CaAl_{1.9}Si_{2.1}$ have been deduced, as compared to that of $CaAl_2Si_2$. Such a result is in good agreement with the observations from the Seebeck coefficient.

To provide a concise interpretation for the observed $S(T)$, we analyse the data with an assumption that both electron-like and hole-like carriers contribute to the diffusive thermoelectric power [17]. The change in the slope of S at around 100 K suggests the existence of lighter electron and heavier hole pockets in the band structure of $CaAl_2Si_2$. However, the electrons become heavier and thus dominate the $S(T)$ below about 100 K. Such a scenario appears to be consistent with the calculated band structure of $CaAl_2Si_2$, where the Fermi surface consists of two small hole pockets centred at the Γ point and one electron pocket centred at the M point [4]. Within the two-band model, it allows us to consider a contribution from semiconducting-like holes in addition to a metallic term as a possible explanation for the observed unusual thermoelectric transport behaviour.

For the metallic thermoelectric power contribution, the low temperature carrier diffusion S_e can be expressed as

$$S_e(T) = -\frac{\pi^2 k_B^2 T}{3|e|}\left[\frac{\partial \ln \sigma_e(\varepsilon)}{\partial \varepsilon}\right]_{\varepsilon=\varepsilon_F}, \tag{5}$$

where $\sigma_e(\varepsilon)$ $[= 1 + c_e\varepsilon]$ is the energy dependence of the conductivity within the relaxation time approximation. Here ε is measured from the Fermi level and $c_e > 0$ for electron-like behaviour. For the sake of simplicity, the mean free path of the carriers (ℓ) is assumed to be independent of temperature. For the hole-like band where the conduction is thermally activated, the corresponding S_h is given by

$$S_h = |k_B/e|(E_h/T). \tag{6}$$

Here E_h is the activation energy and is related to the thermally activated conductivity $\sigma_h = \sigma_0 \exp(-E_h/T)$ with σ_0 a constant. Thus, the overall Seebeck coefficient conceives metallic and hole-like bands:

$$S = \frac{\sigma_e}{\sigma_e + \sigma_h} S_e + \frac{\sigma_h}{\sigma_e + \sigma_h} S_h. \tag{7}$$

Using equations (5)–(7), we have obtained reasonable fits to the data of $CaAl_{2-x}Si_{2+x}$ alloys in the higher temperature regime, and the fit for the $CaAl_2Si_2$ compound is demonstrated as a solid line in the upper panel of figure 4. From these fits, we can determine the normalized slope of the linear energy dependence for the metallic band at the Fermi level, $c_e = \mathrm{d} \ln \sigma_e(\varepsilon_F)/\mathrm{d}\varepsilon$, and the activation energy E_h for each composition, with the fitting parameters tabulated in table 1. The extracted activation energy values are approximately 40–70 meV, as required for a contribution

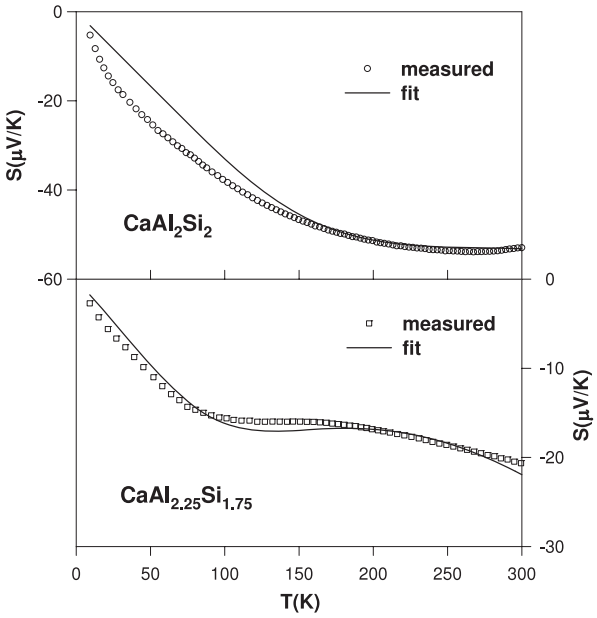

Figure 4. Seebeck coefficient as a function of temperature for $CaAl_2Si_2$ (upper panel) and $CaAl_{2.25}Si_{1.75}$ (lower panel) along with fitting using equations (5)–(7).

to conductivity up to the intermediate temperature range. Further, in order to reproduce the observed slope change for $CaAl_{2.1}Si_{1.9}$ and $CaAl_{2.25}Si_{1.75}$, ε was found to be about 100 meV. The fit along with the measured data of $CaAl_{2.25}Si_{1.75}$ is shown in the lower panel of figure 4. Based on these analyses, a two-band model involving metallic electron and semiconductor-like hole conductions seems to be a reasonable description for the observed $S(T)$.

3.3. Thermal conductivity

The measured thermal conductivity $\kappa(T)$ as a function of temperature (10–300 K) for the studied compositions is shown in figure 5. As the temperature decreases, a gradual increase in κ is followed by a well defined maximum/peak around 50 K and then a steep fall below 50 K. These features are the typical behaviour of solids. In general, the peak height is reduced or suppressed by disorder, defects, and/or impurities. Nevertheless, we have found that a slight excess of Al content results in an increase of the peak height, which is consistent with the resistivity result, which indicates the lowest residual resistivity in $CaAl_{2.1}Si_{1.9}$. Our earlier report on $CoSi_{1-x}Al_x$ alloys has led to a dramatic decrease of the peak height, attributed to the lattice imperfections introduced by the Al substitution [18]. In the present study, replacing a small amount of Si by Al may have the effect of driving the $CaAl_2Si_2$ compound toward a higher carrier density and thus enhancing the metallicity.

The Wiedemann–Franz (WF) law is frequently used to estimate the phonon contribution to the total thermal conductivity by subtracting the electronic contribution $\sigma L_0 T$ from the measured thermal conductivity. Room temperature values of κ_e are given in table 2 and found to be less than 10% of the total thermal conductivity. From the estimated data, one can safely argue that the total thermal conductivity is mainly due to the lattice phonons rather than the charge carriers in these alloys.

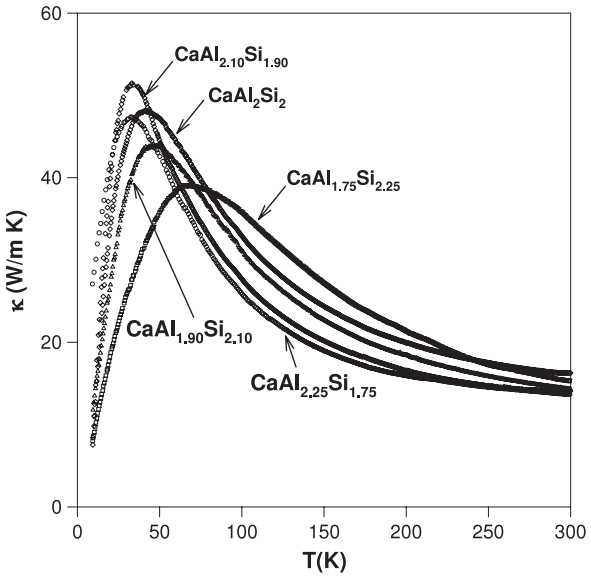

Figure 5. Temperature dependence of thermal conductivity for the $CaAl_{1.75}Si_{2.25}$, $CaAl_{1.9}Si_{2.1}$, $CaAl_2Si_2$, $CaAl_{2.1}Si_{1.9}$, and $CaAl_{2.25}Si_{1.75}$ alloys.

Table 2. Electronic thermal conductivity at room temperature (about 300 K) and fitting parameters of lattice thermal conductivity determined from equations (8) and (9).

Alloys	κ_e (W m^{-1} K^{-1})	L (μm)	P_d (10^{-14} K^{-3})	P_p (10^{-19} s K^{-1})
$CaAl_{1.75}Si_{2.25}$	0.5723	7.40	1.07	1.2
$CaAl_{1.9}Si_{2.1}$	1.3934	7.93	1.25	2.0
$CaAl_2Si_2$	0.4743	4.51	2.13	1.6
$CaAl_{2.1}Si_{1.9}$	1.1362	9.27	0.78	2.0
$CaAl_{2.25}Si_{1.75}$	0.8466	8.64	0.72	2.3

We now proceed to discuss the influence of Al/Si ratio on the phonon scattering processes in these alloys by modelling the T-dependent κ_L within the Debye approximation (Klemens–Callaway model) [18, 19]. The use of the Debye model is reasonable since the temperature region of interest lies well below the Debye temperature. Such an analysis has already been successfully applied to the cobalt monosilicide [19] and other materials [20]. Deduced fitting parameters will reveal information about the phonon scattering mechanisms in the studied samples. The lattice thermal conductivity in the Debye approximation follows the equation

$$\kappa_L = \frac{k_B}{2\pi^2 v}\left(\frac{k_B T}{\hbar}\right)^3 \int_0^{\theta_D/T} \frac{\xi^4 e^\xi}{\tau_p^{-1}(e^\xi - 1)^2}\, d\xi, \tag{8}$$

where $\xi = \hbar\omega/k_B T$ is dimensionless, ω is the phonon frequency, θ_D is the Debye temperature, v is the average phonon velocity, and τ_p^{-1} is the phonon scattering relaxation rate. Here τ_p^{-1} can be represented by the sum of the various contributions for the different scattering channels (Matthiessen's rule) as

$$\tau_p^{-1} = \frac{v}{L} + (P_d/k_B^3)\omega^4\hbar^3 + P_p\omega^2 T e^{(-\theta_D/3T)}, \tag{9}$$

where the grain size L and the coefficients P_d and P_p are the fitting parameters. The terms in equation (9) are the scattering rates for grain-boundary, point defect, and phonon–phonon

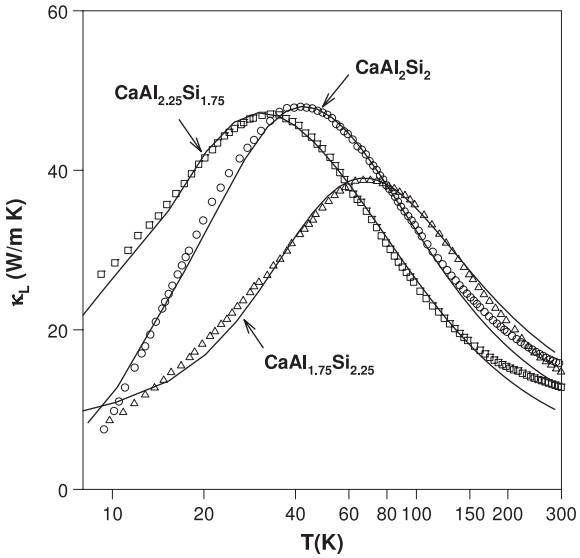

Figure 6. Lattice thermal conductivity for $CaAl_{1.75}Si_{2.25}$, $CaAl_2Si_2$, and $CaAl_{2.25}Si_{1.75}$ versus temperature. The solid lines represent the calculation based on equations (8) and (9).

Umklapp scattering, respectively. Taking $\theta_D = 274$ K determined from the band structure calculation on $CaAl_2Si_2$, we have estimated average phonon velocity $v = 3.44 \times 10^5$ cm s^{-1} following $v = \theta_D(k_B/\hbar)(6\pi^2 n)^{-1/3}$ with n the carrier density. In the calculation of temperature dependent phonon thermal conduction of $CaAl_{2-x}Si_{2+x}$ alloys, we have obtained the parameters that characterize the strengths of the phonon–defect, phonon–grain boundary and phonon–phonon scattering process and these are listed in table 2. The experimental data of all studied samples can be fitted very well in the low temperature range, but deviate from the data points at high temperatures. The selected fitting curves (solid lines) along with the experimental data are drawn in figure 6. The calculated electron–phonon coupling constant of about 0.17 indicates that the electron–phonon interaction is very weak in $CaAl_2Si_2$, in accordance with the band structure calculations [5]. We thus stress that electron–phonon scattering has a minor influence on the lattice thermal conductivity in $CaAl_{2-x}Si_{2+x}$.

As seen from table 2, the Umklapp coefficient P_p scatters around in these samples, presumably due to the unknown Debye temperature for these materials. However, such a discrepancy only affects the fitting result at high temperatures. A close inspection shows that other fitting parameters, the grain size L and the transport coefficient P_d, depend on the Al/Si ratio in a similar manner as observed in the electrical transport properties. It is seen that L (P_d) is the smallest (largest) for the stoichiometric compound among the studied samples, while the obtained values for Al deficient samples are comparable but noticeably smaller (larger) than that of the Al excess samples. The grain-boundary scattering is generally a dominant mechanism for the low-temperature κ_L; however, the point-defect scattering on the other hand has a strong influence on the appearance of the shape and position of the phonon peak occurring in the intermediate-temperature regime. We thus conclude that the variation of lattice thermal conductivity in these ternary silicides is most likely due to the modification of the phonon–point defect scattering mechanism. Such a result may be originated from the mass fluctuations between Al and Si, although their mass difference is less than 4%. A similar observation on the synthetic diamond single crystal versus isotope content has been reported and results have

been quantitatively interpreted by the Klemens–Callaway model [18, 19]. Besides, other lattice imperfections, mainly vacancies, may be introduced via Al/Si substitution, which in turn lead to a substantial number of defects in the non-stoichiometric samples.

4. Conclusions

In conclusion, we have found that altering the Al/Si ratio leads to significant changes in the electronic structure as evidenced by the noticeable composition dependence in the magnitude of S, being consistent with the reported and presently investigated transport properties. The absence of the linear temperature dependence in the Seebeck coefficient indicates unusual metallic behaviour in these compounds. An analysis of the electrical resistivity shows that the high-temperature feature of $CaAl_2Si_2$ could be due to the change in carrier density/mobility as a consequence of the electron correlation. The results of Seebeck coefficient suggest the electrons and holes contribute to the thermoelectric transport, in accordance with the calculated band structure. By fitting the measured thermal conductivity to the given model, various scattering mechanisms and possible mechanisms have been discussed. The current finding indicates the importance of phonon–point defect scattering to the lattice thermal conductivity in these ternary alumino-silicides.

Acknowledgments

The authors would like to thank the National Science Council of Taiwan for financially supporting this research under contract Nos NSC-95-2112-M-259-006 (YKK) and NSC-95-2112-M-006-021-MY3 (CSL).

References

[1] Imai M, Nishida K, Kimura T and Abe H 2002 *Appl. Phys. Lett.* **80** 1019
[2] Lorenz B, Lenzi J, Cmaidalka J, Meng R L, Sun Y Y, Xue Y Y and Chu C W 2002 *Physica* C **383** 191
[3] Imai M, Abe H and Yamada K 2004 *Inorg. Chem.* **43** 5186
[4] Huang G Q 2006 *J. Phys. Conf. Ser.* **29** 73
[5] Huang G Q, Liu M, Chen L F and Xing D Y 2005 *J. Phys.: Condens. Matter* **17** 7151
[6] Lue C S, Xie B X and Fang C P 2006 *Phys. Rev.* B **74** 014505
[7] Nagamatsu J, Nakagawa N, Muranaka T, Zenitani Y and Akimitsu J 2001 *Nature* **410** 63
[8] Lue C S and Kuo Y K 2002 *Phys. Rev.* B **66** 085121
[9] Varshney D and Kaurav N 2004 *Eur. Phys. J.* B **40** 129
[10] Varshney D, Choudhary K K and Singh R K 2002 *Supercond. Sci. Technol.* **15** 1119
[11] Varshney D, Shah S and Singh R K 1998 *Superlattices Microstruct.* **24** 409
[12] Varshney D, Kaurav N and Choudhary K K 2005 *Supercond. Sci. Technol.* **18** 1259
[13] Thompson A H 1975 *Phys. Rev. Lett.* **35** 1786
[14] Lue C S, Kuo Y K, Horng S N, Peng S Y and Cheng C 2005 *Phys. Rev.* B **71** 064202
[15] Kuo Y K, Sivakumar K M, Lin C R, Lue C S and Lin S T 2005 *J. Appl. Phys.* **97** 103717
[16] Lue C S, Wang S Y and Fang C P 2007 Unpublished
[17] Lee J H, Char K, Park Y W, Zhao L Z, Zhu D B, McIntosh G C and Kaiser A B 2000 *Phys. Rev.* B **61** 14815
[18] Lue C S, Kuo Y K, Huang C L and Lai W J 2004 *Phys. Rev.* B **69** 125111
[19] Kuo Y K, Sivakumar K M, Huang S J and Lue C S 2005 *J. Appl. Phys.* **98** 123510
[20] Onn D G, Witek A, Qiu Y Z, Anthony T R and Banholzer W F 1992 *Phys. Rev. Lett.* **68** 2806